Published in final edited form as:
Eur J Med Chem. 2010 December ; 45(12): 5781–5791. doi:10.1016/j.ejmech.2010.09.038.

Synthesis and biological evaluation of 2-(3′,4′,5′-trimethoxybenzoyl)-3-aryl/arylaminobenzo[*b*]thiophene derivatives as a novel class of antiproliferative agents

Romeo Romagnoli[a,*], **Pier Giovanni Baraldi**[a], **Carlota Lopez Cara**[a], **Ernest Hamel**[b], **Giuseppe Basso**[c], **Roberta Bortolozzi**[c], and **Giampietro Viola**[c,**]

[a]Dipartimento di Scienze Farmaceutiche, Università di Ferrara, Via Fossato di Mortara 17-19, 44100 Ferrara, Italy

[b]Screening Technologies Branch, Developmental Therapeutics Program, Division of Cancer Treatment and Diagnosis, National Cancer Institute at Frederick, National Institutes of Health, Frederick, MD 21702, USA

[c]Dipartimento di Pediatria, Laboratorio di Oncoematologia, Università di Padova, 35131 Padova, Italy

Abstract

The biological importance of microtubules in mitosis, as well as in interphase, makes them an interesting target for the development of anticancer agents. Small molecules such as benzo[*b*]thiophenes are attractive as inhibitors of tubulin polymerization. Thus, a new class of compounds that incorporated the structural motif of the 2-(3′,4′,5′-trimethoxybenzoyl)-3-aryl/arylamino benzo[*b*]thiophene molecular skeleton, with electron-donating (Me, OMe, SMe or OEt) or electron-withdrawing (F and Cl) substituents on the B-ring, was synthesized and evaluated for antiproliferative activity, inhibition of tubulin polymerization and cell cycle effects. The most promising compound in this series was 2-(3′,4′,5′-trimethoxybenzoyl)-3-(4′-ethoxyphenyl)-benzo[*b*]thiophene (**4e**), which significantly inhibited cancer cell growth at submicromolar concentrations, especially against HeLa and Jurkat cells, and interacted with tubulin. As determined by flow cytometric analysis, **4e** caused G2/M phase arrest and apoptosis in a time-and concentration-dependent manner. The block in G2/M was correlated with increased expression of cyclin B1 and phosphorylation of cdc25c. Moreover, **4e** perturbed mitochondrial membrane potential and caused activation of caspase-3 and cleavage of poly(ADP-rybose)polymerase (PARP), events that are involved in **4e**-induced apoptosis.

Keywords

Microtubules; Benzo[*b*]thiophene; Apoptosis

1. Introduction

The microtubule system of eukaryotic cells plays important roles in regulating cell architecture, and it has an essential role in cell division, since microtubules are a key component of the mitotic spindle [1,2]. Microtubules are a dynamic cellular compartment in

*Corresponding author. Tel.: +39 (0) 532 455303; fax: +39 (0) 532 455953. rmr@unife.it (R. Romagnoli). **Corresponding author. Tel.: +39 (0) 49 8211451; fax: +39 (0) 49 8211462. giampietro.viola.1@unipd.it (G. Viola)..

both neoplastic and normal cells. This dynamicity is characterized by the continuous turnover of αβ-tubulin heterodimers in the polymeric microtubules. They are involved in a variety of fundamental cellular processes, such as regulation of motility, cell signaling, formation and maintenance of cell shape, as well as transport of material within the cell [3–5]. Numerous chemically diverse antimitotic agents, many of which are derived from natural products, have been found to interact specifically with tubulin [6–13].

Among the natural microtubule depolymerizing agents, combretastatin A-4 (CA-4, **1**; Chart 1) is one of the more studied compounds. CA-4, isolated from the bark of the South African tree *Combretum caffrum* [14], strongly inhibits the polymerization of tubulin by binding to the colchicine site [15]. Because of its structural simplicity, a wide number of CA-4 analogues have been developed and evaluated in structure–activity relationship (SAR) studies [16–18].

Although many synthetic tubulin inhibitors have been synthesized in the last few years, there is still a need to identify novel molecules that target microtubules. Such compounds would ideally be characterized by relatively simple structures and be easy to prepare in a cost-effective way. Among such compounds, the benzo[*b*]thiophene molecular skeleton is the core structure of a series of derivatives with general structure **2** described by Pinney et al. [19]. These compounds are based on the 2-aryl-3-(3′,4′,5′-trimethoxybenzoyl)-benzo[*b*]thiophene ring system and showed antiproliferative activity ranging from 0.5 to 2 μM against human Burkitt lymphoma, CA-46 and human breast carcinoma MCF-7 cells. Compound **2a** showed partial effect on tubulin polymerization at a concentration of 40 μM, while **2b** was active at a lower concentration (IC_{50} = 3.5 μM) [19,20]. These findings prompted us to study this class of compounds in more detail.

In this article we present a flexible, concise and highly convergent protocol for the preparation of two new series of derivatives with general structure **3** and **4**, characterized by the presence of a substituted aryl or arylamino moiety, respectively, on the 3-position of the 2-(3′,4′,5′-trimethoxybenzoyl)benzo[*b*]thiophene core.

In the present investigation, the 3′,4′,5′-trimethoxyphenyl group on the 2-benzoyl moiety was kept unchanged because it is the characteristic structural requirement for activity in a numerous inhibitors of tubulin polymerization, such as colchicine, CA-4 and podophyllotoxin [17,21,22]. The pharmacological evaluation of compounds **3a–k** and **4a–e** allowed us to investigate SAR when electron-withdrawing (F and Cl) or electron-releasing (Me, MeO, MeS and EtO) substituents were placed on the B-ring at the 3-position of the benzo[*b*]thiophene ring.

Finally, by the synthesis of compounds **4fg** we evaluated the effect of the introduction of the electron-releasing methyl group at the 6-position of the C-ring of the benzo[*b*]thiophene nucleus.

2. Chemistry

The 2-(3′,4′,5′-trimethoxybenzoyl)-3-aryl/arylamino benzo[*b*] thiophene derivatives **3a–k** and **4a–g** were synthesized by the procedure reported in Scheme 1. 2-Mercaptobenzonitrile **7a** [23] and 5-methyl-2-mercaptobenzonitrile **7b** were obtained by S-debenzylation of thioethers **6a** and **6b**, respectively, with aluminium chloride in benzene. These latter derivatives were obtained in good yields by condensation of the corresponding 2-nitrobenzonitriles **5a** and **5b** with the potassium salt of phenyl methanethiol in cold aqueous DMF [24]. The 3-amino-2-(3,4,5-trimethoxybenzoyl)benzo[*b*]thiophenes **8ab** were prepared in excellent yields by a “one-pot” cyclization reaction of 2-cyanothiophenol **7a** and 5-methyl-2-mercaptobenzonitrile **7b**, respectively, with 1-(3,4,5-trimethoxyphenyl)-2-bromo-

ethanone and anhydrous potassium carbonate in refluxing acetone. The precursors 3-bromobenzo[*b*]thiophenes **9ab** were prepared from the corresponding 3-amino counterparts **8ab** by treatment with *tert*-butyl nitrite (*t*BuONO) and copper (II) bromide ($CuBr_2$) in acetonitrile [25]. The 3-aryl benzo[b]thiophenes **3a–k** were synthesized from the key intermediate **9a** by a standard Suzuki cross-coupling reaction with appropriate aryl boronic acids under heterogeneous conditions [$Pd(PPh_3)_4$, K_2CO_3] in refluxing toluene [26]. The 3-arylaminobenzo[*b*]thiophenes **4a–e** and **4–g** were prepared in good yield by palladium-catalyzed amination of the appropriate 3-bromobenzo[*b*]thiophene **9a** and **9b**, respectively, with the corresponding aniline in the presence of palladium (II) acetate ($Pd(OAc)_2$), rac-2,2′-bis-(diphenylphosphane)-1,1′-binaphtyl (BINAP) and cesium carbonate ($CsCO_3$) in toluene [27,28].

3. Biological results and discussion

Table 1 summarizes the growth inhibitory effects of 2-(3′,4′,5′-trimethoxy)benzo[*b*]thiophene derivatives **3a–j** and **4a–g** against a panel of five human cell lines, which were derived from different cancer types, including cervix carcinoma (HeLa), non-small lung carcinoma (A549), promyelocytic leukemia (HL-60), T-leukemia (Jurkat) and chronic myelogenous leukemia (K562) cells. All of the compounds showed a considerable growth inhibitory effect and were active in the micromolar range, although the differences between the different cell lines are not significant. Of all tested compounds, the 3-(4′-ethoxyphenylamino) derivative **4e** possessed the highest potency, inhibiting the growth of HeLa, A549, HL-60, Jurkat and K562 cells with IC_{50} values of 0.7, 1.4, 0.5, 0.3 and 0.2 μM, respectively. These values are from 2- to 15-fold lower than those obtained with the 3-(4-ethoxyphenyl) derivative **3k**. Starting from **4e**, the introduction of a C-6 methyl on the C-ring (compound **4g**) has a detrimental effect on activity, with **4g** being 4- to 20-fold less potent than **4e**.

In comparing compounds with the same substituent on the B-ring (**3a** *vs*. **4a, 3c** *vs*. **4b, 3d** *vs*. **4c, 3e** *vs*. **4d, 3k** *vs*. **4e**)interms of the average IC_{50}, in two cases (the unsubstituted **3a** and the *para*-methoxy substituted **3e**) the aryl derivative was more active than the 3-anilino derivatives. In contrast, the 3-anilino derivatives **4b**, **4c** and **4e**, with *para*-chloro, *para*-methyl and *para*-ethoxy substituents, respectively, were more active than the corresponding aryl derivatives. The 3-phenyl derivative **3a** exhibited good antiproliferative activity against HeLa, HL-60, Jurkat and K562 cells (IC_{50} 1.5–2.1 μM) and moderate potency against A549 cells (IC_{50} = 5 μM).

In the series of 3-aryl analogues **3b–**, the *para*-substituted phenyl derivatives with either electron-withdrawing groups, such as fluorine (**3b**) or chlorine (**3c**), or an electron-donating group, like methyl (**3d**), methoxy (**3e**), thiomethyl (**3f**) or ethoxy (**3k**), exhibited good antiproliferative activities, with average IC_{50} values of 2.7–4.8 μM. Introducing an electron-withdrawing fluorine (**3b**)or chlorine (**3c**) led to reduction in antiproliferative activity in comparison with the unsubstituted derivative **3a**, with the chlorine having a greater effect than the fluorine atom (2-fold increased activity against HeLa, A549, Jurkat and K562 cells). Replacement of chlorine with electron-donating methyl group retained the activity toward A549, Jurkat and K562 cells, while a 1.5- and 2-fold increased activity against HeLa and HL-60 cells were observed.

Electron-donating groups also caused a loss of activity relative to **3a**, with the least effects occurring with *para* thiomethyl and methoxy groups (**3e** and **3f**, respectively). Moving the methoxy group from *para*-(**3f**) to the *ortho*-position (**3g**) caused about a 50% loss in average antiproliferative activity, as did addition of a second methoxy group at the *ortho*-position

(**4h**). Still larger losses in activity occurred with addition of a *meta*-methyl group (**3j**) or with two methoxy groups in the *ortho* and *meta* positions (**3i**).

In the series of 3-anilino derivatives **4a–g**, average antiproliferative activity was more dependent on the substituent on the B-phenyl ring at the 3-position, there being a 9-fold difference between **4e**, the most active compound in the group, and **4d**, the least active.

Relative to the unsubstituted **4a**, the electron-withdrawing chlorine (**4b**), had essentially no effect, while the different electron-donating groups had variable effects. Thus, the *para*-methyl group (**4c**) had minimal effect, the *para*-methoxy group (**4d**) led to almost a 50% loss in activity, and the *para*-ethoxy group (**4e**) to a 5-fold increase in activity. One further modification we explored in the 3-anilino derivatives was addition of a methyl substituent in ring C, at the 6-position of the benzo[*b*]thiophene skeleton. Again the effect was variable. With a *para*-methyl substituent on the B-ring, the C-ring methyl enhanced activity against HL-60 and HeLa cells (cf. **4f** with **4c**). In contrast, with the *para*-ethoxy substituent, the C-ring methyl group led to almost from 4-to 20-fold loss of activity (cf. **4g** with **4e**).

To investigate whether the antiproliferative activities of these compounds were related to an interaction with the microtubule system, representative compounds **4e**, **4f** and **4g**, were evaluated for their effects on tubulin polymerization [29]. For comparison, CA-4 was examined in contemporaneous experiments as a reference compound. The benzo[*b*]thiophene derivatives **4e** and **4f** inhibited the assembly reaction with IC_{50} values of 7.2 and 15 μM, respectively, considerably higher than the value obtained with CA-4 (IC_{50} = 1.0 μM). Compound **4g**, however, did not inhibit the reaction by 50% even 40 μM. These results indicate that tubulin may be the intracellular target of compounds **4e** and **4f**. Nevertheless, we could not exclude the possibility that these compounds may affect other molecular targets in addition to microtubules resulting in the enhanced cytotoxicity.

3.1. Compound 4e induces G2/M phase arrest and changes the expression of G2/M regulatory proteins

Because molecules exhibiting effects on tubulin assembly should cause alteration of cell cycle parameters with preferential G2/M blockade, flow cytometric analysis was performed to determine the effect of different concentrations of the most active compound **4e** on leukemia T-cell Jurkat (Fig. 1A) and HeLa cells (Fig. 1B). Cellular DNA was stained with propidium iodide (PI) for these studies.

Untreated Jurkat cells showed a classic pattern of proliferating cells distributed between the G1 (58%), S (36%) and G2/M (15%) phases. With **4e** treatment, a clear G2/M arrest pattern occurred in a concentration-dependent manner, with a concomitant decrease of cells in the other phases of the cell cycle. In particular, as showed in Fig. 1 (panel A), the G2/M cell population increased from 15% in the control to 70% with compound **4e** at 1.25 μM. Under the same conditions, the G1 cells decreased from 58 in the control to 10% and the S phase cells decreased from 36 to 18%.

In the HeLa cells, the G2/M block induced by **4e** was even more pronounced (Fig. 1 panel B). At 0.625 μM, 52% of the cells were blocked in G2/M, and this increased further to 85% at 1.25 μM, with accompanying reductions of cells in the G1 and S phases. After 48 h of treatment, a hypodiploid peak (sub-G1) indicative of apoptosis, appeared in both cell lines (data not shown).

We next studied the association between **4e**-induced G2/M arrest and alterations in expression of proteins that regulate cell division. Generally, antimitotic drugs directed against tubulin, cause cell arrest at the prometaphase/metaphase to anaphase transition,

which is normally regulated by the mitotic checkpoint [30]. In eukaryotic cells, cyclin B and cdc25c kinase regulate the onset of the G2/M phase. Phosphorylation of cdc25c directly stimulates its phosphatase activity, and this is necessary to activate cyclin B kinase on entry into mitosis [31].

As shown in Fig. 2 in HeLa cells, **4e** causes a concentration-dependent increase in cyclin B1 expression, while slower migrating forms of phosphatase cdc25c were present, indicating changes in the phosphorylation state of this protein. These changes are consistent with the observed cell cycle arrest in mitosis.

The tumor suppressor protein p53 acts as a DNA binding transcription factor, regulating specific target genes to arrest the cell cycle and initiate apoptosis. However, with increasing concentrations of **4e**, there was no difference in the expression of p53. This suggests that cell growth inhibition and apoptosis induced by **4e** may be through a p53-independent pathway.

3.2. Analysis of cell death

To characterize the mode of cell death induced by **4e**, a biparametric cytofluorimetric analysis was performed using PI, which stains DNA and is permeable only to dead cells, and fluorescent immunolabeling of the protein annexin-V, which binds to the phospholipid phosphatidylserine (PS) in a highly selective manner [32,33].

This phospholipid flips from the inner to the outer leaflet of the plasma membrane during apoptosis. Positive staining with annexin-V correlates with the loss of plasma membrane polarity, but this staining precedes the complete loss of membrane integrity that accompanies the later stages of cell death, resulting from either apoptosis or necrosis. In contrast, PI can only enter cells after complete loss of membrane integrity. Thus, dual staining for annexin-V and with PI permits discrimination between unaffected cells (annexin-V^-/PI^-), early apoptotic cells (annexin-V^+/PI^-), late apoptotic cells (annexin-V^+/PI^+) and necrotic cells (annexin-V^-/PI^+) [33]. Fig. 3 (panel A) shows representative, biparametric histograms demonstrating the effects of different concentrations of **4e** on HeLa cells after 24 h of treatment. Compound **4e** at 24 h had already induced an accumulation of annexin-V positive cells in comparison with the control, and this accumulation was concentration-dependent. There was a further increase in these apoptotic and necrotic cells at 48 h.

These findings led us to us to investigate further apoptotic pathways following treatment with **4e**.

3.3. Mitochondrial depolarization and generation of reactive oxygen species (ROS)

Mitochondria play a key role in the apoptotic process, and it is well established that at an early stage apoptotic stimuli alter the mitochondrial potential ($\Delta\Psi_{mt}$) [34,35]. Rhodamine 123 (Rho 123) was used as an indicator of mitochondrial membrane potential [36] analyzing, by flow cytometry, HeLa cells after treatment with compound **4e**. As shown in Fig. 4 (panel A), the test compound induced in a concentration and time dependent manner a reduction of Rho 123 fluorescence intensity, which reflects the collapse of $\Delta\Psi_{mt}$.

Mitochondrial membrane depolarization is associated with mitochondrial production of ROS [37]. Therefore, we investigated whether ROS production increased after treatment with the test compounds. We utilized the fluorescence indicator hydroethidine (HE), whose fluorescence appears if ROS are generated [38,39]. HE is oxidized by superoxide anion into the ethidium ion, which fluoresces red. Superoxide is produced by mitochondria due to a shift from the normal 4-electron reduction of O_2 to a 1-electron reduction when cytochrome c is released from mitochondria. ROS generation was also measured with the dye 2,7-

dichlorodihydro-fluorescein diacetate (H_2-DCFDA), which is oxidized to the fluorescent compound dichlorofluorescein (DCF) by a variety of peroxides including hydrogen peroxide [39].

The results are presented in Fig. 3 (panels B and C), where it can be observed that **4e** induces the production of large amounts of ROS in comparison with control cells, which agrees with the previously described dissipation of $\Delta\Psi_{mt}$.

3.4. Caspase activation and PARP cleavage

The mechanism by which apoptosis is induced by antimitotic drugs is not completely understood [30]. The activation of caspases represent a crucial step in the induction of drug induced apoptosis and cleavage of poly(ADP-ribose)polymerase (PARP) by caspase-3 is considered to be one of the hallmarks of apoptosis [40–43]. As shown in Fig. 5 (panel A), incubation of HeLa cells with compound **4e** resulted in the activation of caspase-3 in a time- and concentration-dependent manner. In agreement with this finding, immunoblot analysis (Fig. 5, panel B) showed that the typical 89 kDa cleaved fragment of PARP increased in treated cells with compound **4e** after 24 h and especially after 48 h of treatment.

Bcl-2 is a protein that has been extensively investigated as a modulating agent of apoptosis and plays a major role as an inhibitor of apoptosis. It does this by regulating the mitochondrial membrane potential, thus avoiding release of cytochrome *c* and caspase activation [44]. Another protein involved in the apoptosis pathways is Bax, which has been shown to promote apoptosis and increases the sensitivity of cancer cells to a variety of antineoplastic agents [45]. Therefore, we examined whether the induction of apoptosis by **4e** was associated with changes in the expression of these proteins. As shown in Fig. 5 (panel B) by immunoblot analysis, treatment with **4e** resulted in a slight decrease in the expression of Bcl-2 while the expression of Bax remained unchanged.

Altogether these data indicate that the induction of apoptosis by **4e** is associated with Bcl-2 down regulation and caspase-3 activation, which in turn stimulates PARP cleavage.

4. Conclusions

In this report we have described a procedure that gives access to a range of substitution patterns at the 3-position of the benzo[*b*] thiophene ring, making it an ideal process for SAR studies of biologically active molecules. In the series of 3-aryl derivatives **3a–k**, the introduction both of electron-releasing or electron-withdrawing groups on the B-ring did not have a profound effect on the activity in comparison with the unsubstituted 3-aryl derivative **3a**. This study revealed that 2-(3′,4′,5′-trimethoxybenzoyl) 3-substituted benzo[*b*] thiophenes are an interesting class of compounds, and our SAR study showed that **4e** was the most active agent among those synthesized, since **4e** had antiproliferative activity in the submicromolar range against HeLa, HL-60, Jurkat and K562 cells. The introduction of a methyl group at the C-6 position of benzo[*b*]thiophene core was detrimental to antiproliferative activity. We also showed that the antiproliferative activity of **4e** and **4f** may derive from an interference with microtubule assembly, although at this stage we cannot exclude that other molecular targets could be involved in the mechanism of action of these compounds. The interaction with tubulin leads to cell cycle arrest in the G2/M phase. Consistent with the mitotic block, treatment of HeLa cells led to increased expression of cyclin B1, which then phosphorylated cdc25c. We also found that mitotic arrest caused by **4e** was associated with the induction of apoptosis, as manifested by loss of mitochondrial membrane potential, generation of ROS and activation of caspase-3 with typical cleavage of PARP.

5. Experimental protocols

5.1. Chemistry

5.1.1. Materials and methods—^{1}H NMR spectra were recorded on a Bruker AC 200 spectrometer. Chemical shifts (δ) are given in ppm upfield from tetramethylsilane as internal standard, and the spectra were recorded in appropriate deuterated solvents, as indicated. Melting points (mp) were determined on a Buchi-Tottoli apparatus and are uncorrected. All products reported showed ^{1}H NMR spectra in agreement with the assigned structures. Elemental analyses were conducted by the Microanalytical Laboratory of the Chemistry Department of the University of Ferrara. All reactions were carried out under an inert atmosphere of dry nitrogen, unless otherwise described. Standard syringe techniques were applied for transferring dry solvents. Reaction courses and product mixtures were routinely monitored by TLC on silica gel (precoated F_{254} Merck plates) and visualized with aqueous $KMnO_4$. Flash chromatography was performed using 230–400 mesh silica gel and the indicated solvent system. Organic solutions were dried over anhydrous Na_2SO_4. Compounds **5a** and **5b** are commercially available.

5.1.2. Synthesis of 2-benzylsulfanyl-4-methylbenzonitrile (6b)—To a cold solution (ice bath) containing 4-methyl-2-nitro benzonitrile **5b** (3.24 g, 20 mmol) and benzylmercaptan (2.48 g, 20 mmol) in 20 mL of DMF was added dropwise a solution of KOH (2 g, 36 mmol) in 5 mL of water. The mixture was stirred at 4 °C for 2 h and then poured into ice water. The solid was collected, washed with cold water (50 mL), dried in vacuo over P2^{O}5 and recrystallized from petroleum ether, to furnish **6b** as a yellow solid. Yield: 72%, mp 88–90 °C ^{1}H NMR ($CDCl_3$) δ: 2.33 (s, 3H), 4.20 (s, 2H), 7.05 (d, *J* = 7.6 Hz, 1H), 7.16 (s, 1H), 7.28 (m, 5H), 7.49 (d, *J* = 8.0 Hz, 1H).

5.1.3. Synthesis of 2-mercapto-4-methylbenzonitrile (7b)—A solution of **6b** (4.78 g, 20 mmol) in dry benzene (40 mL) was added dropwise over 30 min to a suspension of finely powdered anhydrous aluminium chloride (4.5 g, 33 mmol) in dry benzene (40 mL), and the mixture was stirred under nitrogen at room temperature for 48 h. The green–brown mixture was decomposed by the cautious addition of ice water (100 mL), and the organic layer was separated and washed successively with water (50 mL) and 5% aqueous sodium hydroxide (2 × 50 mL). The alkaline extracts were acidified and extracted with dichloromethane (3 × 50 mL). The organic extracts were washed with brine, dried and evaporated to yield compound **7b** a yellow solid, yield 68%; mp 38–40 °C ^{1}H NMR (DMSO-d_6) δ: 2.36 (s, 3H), 4.02 (s, 1H), 7.00 (d, *J* = 8.8 Hz, 1H), 7.22 (s, 1H), 7.49 (d, *J* = 8.0 Hz, 1H).

5.1.4. General procedure (A) for the synthesis of 2-(3′,4′,5′-trimethoxybenzoyl)-3-amino benzo[b]thiophenes (8ab)—To a solution of **7ab** (1 mmol) in dry acetone (15 mL) was added 2-bromo-1-(3,4,5-trimethoxyphenyl)-ethanone (289 mg, 1 mmol) and anhydrous potassium carbonate (276 mg, 2 mmol) while stirring, and the reaction mixture was refluxed for 18 h. After cooling, the solvent was evaporated, and the residue was dissolved in a mixture of dichloromethane (15 mL) and water (5 mL). The organic layer was washed with brine, dried and evaporated to obtain a residue, which was purified by flash column chromatography. The final product was precipitated from petroleum ether.

5.1.4.1. 2-(3,4,5-Trimethoxybenzoyl)-3-aminobenzo[b]thiophene (8a): The crude residue purified by flash chromatography using ethyl acetate:petroleum ether 3:7 (v:v) as eluent furnished **8a** as a yellow solid (93% yield); mp 148–150 °C. ^{1}H NMR($CDCl_3$) δ: 3.93 (s,

3H), 3.94 (s, 6H), 7.02 (bs, 2H), 7.21 (s, 2H), 7.42 (d, *J* = 7.6 Hz, 1H), 7.51 (d, *J* = 7.2 Hz, 1H), 7.76 (dd, *J* = 7.2 and 7.6 Hz, 2H).

5.1.4.2. 2-(3,4,5-Trimethoxybenzoyl)-3-amino-6-methylbenzo[b] thiophene (8b): The crude residue purified by flash chromatography using ethyl acetate:petroleum ether 3:7 (v:v) as eluent furnished **8b** as a yellow solid (78% yield); mp 128–130 °C. ^{1}H NMR ($CDCl_3$) δ: 2.49 (s, 3H), 3.93 (s, 3H), 3.94 (s, 6H), 7.01 (bs, 2H), 7.20 (s, 2H), 7.22 (d, *J* = 8.0 Hz, 1H), 7.51 (s, 1H), 7.62 (d, *J* = 8.0 Hz, 1H).

5.1.5. General procedure (B) for the synthesis of (3-bromobenzo[b] thiophen-2-yl)(3,4,5-trimethoxyphenyl)methanones (9ab)—To a dry three-necked round-bottom flask, anhydrous $CuBr_2$ (268 mg, 1.2 mmol) and *tert*-butyl nitrite (180 μL, 1.5 mmol) were dissolved in anhydrous acetonitrile (5 mL) under an argon atmosphere. The resulting mixture was warmed at 65 °C and derivative **8ab** (1 mmol) in acetonitrile (3 mL) was slowly added. The reaction was complete after 2 h, as monitored by TLC (EtOAc–petroleum ether 2–8, v/v). The dark mixture was allow to reach room temperature, poured in a 0.1 N aqueous HCl solution (10 mL) and extracted with EtOAc (20 mL). The organic phase was washed twice with 0.1 N aqueous HCl solution (5 mL), brine (5 mL), dried over Na_2SO_4 and concentrated at reduced pressure to furnish a residue that was purified by flash chromatography on silica gel (EtOAc–petroleum ether 1.5–8.5).

5.1.5.1. (3-Bromobenzo[b]thiophen-2-yl)(3,4,5-trimethoxyphenyl) methanone (9a): Following general procedure B, the product was isolated as a purple solid, yield: 85%, mp 105–106 °C ^{1}H NMR ($CDCl_3$) δ: 3.90 (s, 6H), 3.92 (s, 3H), 7.22 (s, 2H), 7.55 (m, 2H), 7.86 (dd, *J* = 6.0 and 3.0 Hz, 1H), 7.98 (dd, *J* = 7.4 and 1.0 Hz, 1H).

5.1.5.2. (3-Bromo-6-methylbenzo[b]thiophen-2-yl)(3,4,5-trimethoxyphenyl)methanone (9b): Following general procedure B, the product was isolated as a purple solid, yield: 67%, mp 130–131 °C ^{1}H NMR ($CDCl_3$) δ: 2.54 (s, 3H), 3.89 (s, 6H), 3.93 (s, 3H), 7.20 (s, 2H), 7.33 (d, *J* = 8.4 Hz, 1H), 7.66 (d, *J* = 0.8 Hz, 1H), 7.86 (dd, *J* = 8.4 Hz, 1H).

5.1.6. General procedure (C) for the preparation of compounds (3a–j)—A mixture of benzo[*b*]thiophene derivative **9a** (0.5 mmol), potassium carbonate (104 mg, 0.75 mmol, 1.5 equiv), the appropriate aryl boronic acid (1 mmol, 2 equiv) and tetrakis (triphenylphosphine)palladium (13.5 mg, 0.012 mmol) in dry toluene (10 mL) was stirred at 100 °C under nitrogen for 18 h, cooled to ambient temperature and evaporated in vacuo. The residue was dissolved with dichloromethane (20 mL), and the resultant solution was washed sequentially with a 2 M aqueous K_2CO_3 solution (5 mL), water (5 mL) and brine (5 mL). The organic layer was dried, filtered and evaporated, and the residue was purified by flash chromatography on silica gel.

5.1.6.1. (3,4,5-Trimethoxyphenyl)(3-phenylbenzo[b]thiophen-2-yl) methanone (3a): Following general procedure C, the residue was purified by chromatography on silica gel (EtOAc–petroleum ether 1.5–8.5) to furnish compound **3a** as a yellow oil, yield: 57%. ^{1}H NMR ($CDCl_3$)δ: 3.76 (s, 6H), 3.81 (s, 3H), 6.92 (s, 2H), 7.27 (m, 5H), 7.48 (m, 2H), 7.82 (dd, *J* = 7.4 and 1.0 Hz, 1H), 7.94 (dd, *J* = 7.4 and 1.0 Hz, 1H). Anal. calcd for $C_{24}H_{20}O_4S$: C, 71.27; H, 4.98; found: C, 71.03; H, 4.69.

5.1.6.2. (3-(4-Fluororophenyl)benzo[b]thiophen-2-yl)(3,4,5-trimethoxyphenyl)methanone (3b): Following general procedure C, the residue was purified by chromatography on silica gel (EtOAc–petroleum ether 1.5–8.5) to furnish compound **3b** as a pink oil, yield: 63%. ^{1}H NMR ($CDCl_3$)δ: 3.77 (s, 6H), 3.84 (s, 3H), 6.95

(s, 2H), 7.04 (d, *J* = 8.8 Hz, 2H), 7.32 (m, 2H), 7.51 (m, 2H), 7.74 (dd, *J* = 7.4 and 1.0 Hz, 1H), 7.97 (dd, *J* = 7.4 and 1.0 Hz, 1H). Anal. calcd for $C_{24}H_{19}FO_4S$: C, 68.23; H, 4.53; found: C, 67.95; H, 4.38.

5.1.6.3. (3-(4-Chlorophenyl)benzo[b]thiophen-2-yl)(3,4,5-trimethoxyphenyl)methanone (3c): Following the general procedure C, the residue purified by chromatography on silica gel (EtOAc–petroleum ether 1.5–8.5) to furnish compound **3c** as a yellow oil, yield: 61%. ^{1}H NMR ($CDCl_3$)δ: 3.78 (s, 6H), 3.85 (s, 3H), 6.76 (s, 2H), 7.24 (m, 2H), 7.49 (m, 4H), 7.82 (dd, *J* = 7.4 and 1.0 Hz, 1H), 7.94 (dd, *J* = 7.4 and 1.0 Hz, 1H). Anal. calcd for $C_{24}H_{19}ClO_4S$: C, 65.67; H, 4.36; found: C, 65.47; H, 4.18.

5.1.6.4. (3,4,5-Trimethoxyphenyl)(3-p-tolylbenzo[b]thiophen-2-yl) methanone (3d): Following general procedure C, the residue was purified by chromatography on silica gel (EtOAc–petroleum ether 2–8) to furnish compound **3d** as a yellow oil, yield: 62%. ^{1}H NMR ($CDCl_3$)δ: 2.04 (s, 3H), 3.76 (s, 6H), 3.81 (s, 3H), 6.94 (s, 2H), 7.10 (d, *J* = 7.4 Hz, 2H), 7.22 (d, *J* = 7.4 Hz, 2H), 7.48 (m, 2H), 7.82 (dd, *J* = 7.2 and 1.0 Hz, 1H), 7.94 (dd, *J* = 7.2 and 1.0 Hz, 1H). Anal. calcd $C_{25}H_{22}O_4S$: C, 71.75; H, 5.30; found: C, 71.58; H, 5.13.

5.1.6.5. (3-(4-Methoxyphenyl)benzo[b]thiophen-2-yl)(3,4,5-trimethoxyphenyl)methanone (3e): Following general procedure C, the residue was purified by chromatography on silica gel (EtOAc–petroleum ether 2–8) to furnish compound **3e** as a yellow oil, yield: 56%. ^{1}H NMR ($CDCl_3$)δ: 3.76 (s, 6H), 3.77 (s, 3H), 3.81 (s, 3H), 6.79 (d, *J*=8.6 Hz, 2H), 6.93 (s, 2H), 7.22 (d, *J* = 8.6 Hz, 2H), 7.47 (m, 2H), 7.82 (dd, *J* = 7.4 and 1.0 Hz, 1H), 7.96 (dd, *J* = 7.4 and 1.0 Hz, 1H). Anal. calcd for $C_{25}H_{22}O_5S$: C, 69.11; H, 5.10; found: C, 68.89; H, 4.89.

5.1.6.6. (3,4,5-Trimethoxyphenyl)(3-(4-(methylthio)phenyl)benzo[b] thiophen-2-yl)methanone (3f): Following general procedure C, the residue was purified by chromatography on silica gel (EtOAc–petroleum ether 1.5–8.5) to furnish compound **3f** as a yellow solid, yield: 62%, mp 91–92 °C ^{1}H NMR ($CDCl_3$)δ: 3.77 (s, 9H), 3.83 (s, 3H), 6.94 (s, 2H), 7.16 (d, *J* = 8.6 Hz, 2H), 7.24 (d, *J* = 8.6 Hz, 2H), 7.47 (m, 2H), 7.82 (dd, *J*= 7.4 and 1.2 Hz, 1H), 7.96 (dd,*J* = 7.4 and 1.2 Hz, 1H). Anal. calcd for $C_{25}H_{22}O_4S_2$: C, 66.64; H, 4.92; found: C, 66.41; H, 4.69.

5.1.6.7. (3-(2-Methoxyphenyl)benzo[b]thiophen-2-yl)(3,4,5-trimethoxyphenyl)methanone (3g): Following general procedure C, the residue was purified by chromatography on silica gel (EtOAc–petroleum ether 2–8) to furnish compound **3g** as a yellow oil, yield: 45%. ^{1}H NMR ($CDCl_3$)δ: 3.75 (s, 6H), 3.78 (s, 3H), 3.79 (s, 3H), 6.79 (d, *J*=8.2 Hz, 1H), 6.86 (dd, *J*=8.6 and 1.0Hz,1H), 6.93 (s, 2H), 7.24 (m, 2H), 7.42 (m, 2H), 7.64 (dd, *J* = 7.2 and 0.8 Hz,1H), 7.91 (dd, *J* = 7.4 and 1.0 Hz, 1H). Anal. calcd for $C_{25}H_{22}O_5S$: C, 69.11; H, 5.10; found: C, 68.88; H, 4.92.

5.1.6.8. (3,4,5-Trimethoxyphenyl)(3-(2,4-dimethoxyphenyl)benzo[b] thiophen-2-yl)methanone (3h): Following general procedure C, the residue was purified by chromatography on silica gel (EtOAc–petroleum ether 2–8) to furnish compound **3h** as a yellow oil, yield: 52%. ^{1}H NMR ($CDCl_3$)δ: 3.76 (s, 3H), 3.79 (s, 3H), 3.81 (s, 6H), 3.84 (s, 3H), 6.72 (d, *J*= 8.4 Hz, 1H), 6.78 (d, *J*= 8.4 Hz, 1H), 6.94 (s, 2H), 7.19 (s, 1H), 7.50 (m, 2H),7.74 (dd, *J*=7.4 and 1.0Hz,1H), 7.90 (dd, *J*=7.4 and 1.0Hz,1H). Anal. calcd for $C_{26}H_{24}O_6S$: C, 67.22; H, 5.21; found: C, 67.02; H, 4.96.

5.1.6.9. (3,4,5-Trimethoxyphenyl)(3-(2,5-dimethoxyphenyl)benzo[b] thiophen-2-yl)methanone (3i): Following general procedure C, the residue was purified by chromatography on silica gel (EtOAc–petroleum ether 4–6) to furnish compound **3i** as a

yellow oil, yield: 49%. ^{1}H NMR ($CDCl_3$)δ: 3.55 (s, 3H), 3.71 (s, 3H), 3.76 (s, 6H), 3.81 (s, 3H), 6.66 (d, *J*=8.4Hz,1H), 6.72 (d, *J*=8.4 Hz,1H), 6.82 (s,1H), 6.94 (s, 2H), 7.44 (m,2H), 7.82(dd, *J*=7.4 and 1.0Hz,1H), 7.94(dd, *J*=7.4 and 1.0Hz,1H). Anal. calcd for $C_{26}H_{24}O_6S$: C, 67.22; H, 5.21; found: C, 66.93; H, 4.98.

5.1.6.10. (3-(4-Methoxy-3-methylphenylamino)benzo[b]thiophen-2-yl)(3,4,5-trimethoxyphenyl)methanone (3j): Following general procedure C, the residue was purified by chromatography on silica gel (EtOAc–petroleum ether 1.5–8.5) to furnish compound **3j** as a yellow oil, yield: 62%. ^{1}H NMR ($CDCl_3$)δ: 2.11 (s, 3H), 3.75 (s, 3H), 3.79 (s, 6H), 3.86 (s, 3H), 6.62 (d, *J* = 7.4 Hz,1H), 6.88 (s, 2H), 7.23 (s,1H), 7.54 (m, 2H), 7.82 (dd, *J* = 7.4 and 1.0 Hz, 1H), 7.92 (dd, *J* = 7.4 and 1.0 Hz,1H), 10.8 (bs, 1H). Anal. calcd for $C_{26}H_{24}O_5S$: C, 69.62; H, 5.39; found: C, 69.47; H, 5.18.

5.1.6.11. (3-(4-Ethoxyphenyl)benzo[b]thiophen-2-yl)(3,4,5-trimethoxyphenyl)methanone (3k): Following general procedure C, the residue was purified by chromatography on silica gel (EtOAc–petroleum ether 2–8) to furnish compound **3k** as a yellow oil, yield: 59%. ^{1}H NMR ($CDCl_3$)δ: 1.38 (t, *J* = 7.2 Hz, 3H), 3.76 (s, 6H), 3.81 (s, 3H), 3.96 (q, *J* = 7.0 Hz, 2H), 6.76 (d, *J* = 6.8 Hz, 2H), 6.92 (s, 2H), 7.22 (d, *J* = 6.8 Hz, 2H), 7.46 (m, 2H), 7.81 (dd, *J* = 7.4 and 1.0 Hz, 1H), 7.92 (dd, *J* = 7.4 and 1.0Hz,1H). Anal. calcd for $C_{26}H_{24}O_5S$: C, 69.62; H, 5.39; found:C, 69.53; H, 5.22.

5.1.7. General procedure (D) for the preparation of compounds (4ag)—A dry Schlenk tube was charged with dry toluene (5 mL), 3-bromobenzo[*b*]thiophene **9ab** (0.5 mmol), $Pd(OAc)_2$ (3 mol%, 15 mg), *rac*-BINAP (4 mol%, 15 mg), $CsCO_3$ (230 mg, 0.7 mmol, 1.4 equiv.) and the appropriate aniline (1 mmol, 2 equiv.) under Ar, and the mixture was heated at 100 °C for 18 h. After cooling, the mixture was filtered on a pad of celite and the filtrate diluted with EtOAc (10 mL) and water (5 mL). The organic phase was washed with brine (5 mL), dried over Na_2SO_4 and concentrated under vacuum. The oil residue was purified by column chromatography on silica gel.

5.1.7.1. (3,4,5-Trimethoxyphenyl)(3-(phenylamino)benzo[b]thiophen-2-yl)methanone (4a): Following general procedure D, the residue was purified by chromatography on silica gel (EtOAc–petroleum ether 1.5–8.5) to furnish compound **4a** as a yellow oil, yield: 53%. ^{1}H NMR ($CDCl_3$)δ: 3.93 (s, 3H), 3.96 (s, 6H), 7.17 (m, 3H), 7.24 (m,6H),7.12 (d, *J* = 7.2 Hz, 1H), 7.92 (m, 1H). 10.7 (bs, 1H). Anal. calcd for $C_{24}H_{21}NO_4S$: C, 68.72; H, 5.05; found: C, 68.52; H, 4.89.

5.1.7.2. (3-(4-Chlorophenylamino)benzo[b]thiophen-2-yl)(3,4,5-trimethoxyphenyl)methanone (4b): Following general procedure D, the residue was purified by chromatography on silica gel (EtOAc–petroleum ether 1.5–8.5) to furnish compound **4b** as a yellow oil, yield: 55%. ^{1}H NMR ($CDCl_3$)δ: 3.93 (s, 3H), 3.95 (s, 3H), 3.96 (s, 3H), 7.12 (d, *J* = 6.8 Hz, 2H), 7.17 (d, *J* = 6.8 Hz, 2H), 7.22 (s, 2H), 7.45 (m, 2H), 7.73 (d, *J* = 8.0 Hz, 1H), 7.92 (d, 8.0 Hz, 1H) 10.6 (bs, 1H). Anal. calcd for $C_{24}H_{20}ClNO_4S$: C, 63.50; H, 4.44; found: C, 63.34; H, 4.17.

5.1.7.3. (3-(p-Tolylamino)benzo[b]thiophen-2-yl)(3,4,5-trimethoxyphenyl)methanone (4c): Following general procedure D, the residue was purified by chromatography on silica gel (EtOAc–petroleum ether 1.5–8.5) to furnish compound **4c** as a yellow solid, yield: 55%, mp 165–166 °C ^{1}H NMR ($CDCl_3$)δ: 2.38 (s, 3H), 3.94 (s, 3H), 3.95 (s, 6H), 7.12 (m, 5H), 7.15 (s, 2H), 7.33 (d, *J*=6.8 Hz,1H), 7.38 (d, *J*=6.8 Hz, 1H), 7.69 (d, *J*=8.2Hz,1H),10.8 (bs, 1H). Anal. calcd for $C_{25}H_{23}NO_4S$: C, 69.26; H, 5.31; found: C, 69.03; H, 5.15.

5.1.7.4. (3-(4-Methoxyphenylamino)benzo[b]thiophen-2-yl)(3,4,5-trimethoxyphenyl)methanone (4d): Following general procedure D, the residue was purified by chromatography on silica gel (EtOAc–petroleum ether 1.5–8.5) to furnish compound **4d** as an orange solid, yield: 65%, mp 159–160 °C ^{1}H NMR ($CDCl_3$)δ: 3.86 (s, 3H), 3.94 (s, 6H), 3.96 (s, 3H), 6.89 (m, 3H), 7.07 (dt, *J* = 7.4 and 1.0 Hz, 1H), 7.24 (m, 4H), 7.40 (dt, *J* = 7.4 and 1.0 Hz, 1H), 7.71 (d, *J* = 8.2 Hz, 1H), 11.0 (bs, 1H). Anal. calcd for $C_{25}H_{23}NO_5S$: C, 66.80; H, 5.16; found: C, 66.59; H, 5.02.

5.1.7.5. (3-(4-Ethoxyphenylamino)benzo[b]thiophen-2-yl)(3,4,5-trimethoxyphenyl)methanone (4e): Following general procedure D, the residue was purified by chromatography on silica gel (EtOAc–petroleum ether 2–8) to furnish compound **4e** as a yellow oil, yield: 62%. ^{1}H NMR ($CDCl_3$)δ: 1.45 (t, *J* = 6.8 Hz, 3H), 3.92 (s, 6H), 3.96 (s, 3H), 4.09 (q, *J* = 6.8 Hz, 2H), 6.88(d, *J* = 8.8 Hz, 1H), 7.12 (d, *J* = 7.8 Hz, 1H), 7.19 (s, 2H), 7.23 (d, *J* = 8.8 Hz, 2H), 7.43 (m, 2H), 7.74 (d, *J* = 7.8 Hz, 1H), 7.92 (m, 1H). 10.9 (bs, 1H). Anal. calcd for $C_{26}H_{25}NO_5S$: C, 67.37; H, 5.44; found: C, 67.13; H, 5.20.

5.1.7.6. (3-(p-Tolylamino)-6-methylbenzo[b]thiophen-2-yl)(3,4,5-trimethoxyphenyl)methanone (4f): Following general procedure D, the was residue purified by chromatography on silica gel (EtOAc–petroleum ether 1.5–8.5) to furnish compound **4f** as a yellow oil, yield: 58%. ^{1}H NMR ($CDCl_3$)δ: 2.38 (s, 3H), 2.42 (s, 3H), 3.92 (s, 3H), 3.96 (s, 6H), 7.12 (m, 4H), 7.17 (s, 2H), 7.34 (d, *J* = 6.8 Hz, 1H), 7.36 (d, *J* = 6.8 Hz, 1H), 7.70 (s, 1H), 10.8 (bs, 1H). Anal. calcd for $C_{26}H_{25}NO_4S$: C, 69.78; H, 5.63; found: C, 69.59; H, 5.35.

5.1.7.7. (3-(4-Ethoxyphenylamino)-6-methylbenzo[b]thiophen-2-yl) (3,4,5-trimethoxyphenyl)methanone (4g): Following general procedure C, the was residue purified by chromatography on silica gel (EtOAc–petroleum ether 2–8) to furnish compound **4g** as an orange solid, yield: 56%, mp 65–66 °C ^{1}H NMR ($CDCl_3$)δ: 1.45 (t, *J* = 7.0 Hz, 3H), 2.41 (s, 3H), 3.94 (s, 6H), 3.96 (s, 3H), 4.07 (q, *J* = 7.0 Hz, 2H), 6.88 (d, *J* = 6.4 Hz, 1H), 7.07 (d, *J* 7.0 Hz, 2H), 7.18 (s, 2H), 7.26 (m, 3H), 7.47 (s, 1H), 10.9 (bs, 1H). Anal. calcd for $C_{27}H_{27}NO_5S$: C, 67.90; H, 5.70; found: C, 67.69; H, 5.49.

5.2. Biological assays

5.2.1. Antiproliferative assays—Human T-leukemia (Jurkat), human promyelocytic leukemia (HL-60) and human chronic myelogenous leukemia (K562) cells were grown in RPMI-1640 medium, (Gibco, Milano Italy). Human non-small lung carcinoma (A549) and human cervix carcinoma (HeLa) cells were grown in DMEM medium (Gibco, Milano, Italy) Both media were supplemented with 115 units/mL of penicillin G (Gibco, Milano, Italy), 115 μg/mL streptomycin (Invitrogen, Milano, Italy) and 10% fetal bovine serum (Invitrogen, Milano, Italy). Individual wells of a 96-well tissue culture microtiter plate were inoculated with 100 μL of complete medium containing 8× 10^3 cells. The plates were incubated at 37 °C in a humidified 5% CO_2 incubator for 18 h prior to the experiments. After medium removal, 100 μL of the drug solution, dissolved in complete medium at different concentrations, was added to each well and incubated at 37 °C for 72 h. Cell viability was assayed by the 3-(4,5-dimethylthiazol-2-yl)-2,5-diphenyl tetrazolium bromide (MTT) test as previously described [46]. The IC_{50} was defined as the compound concentration required to inhibit cell proliferation by 50%.

5.2.2. Effects on tubulin polymerization—To evaluate the effect of the compounds on tubulin assembly *in vitro* [29], varying concentrations were preincubated with 10 μM tubulin in glutamate buffer at 30 °C and then cooled to 0 °C. After addition of GTP, the mixtures were transferred to 0 °C cuvettes in a recording spectrophotometer and warmed to 30 °C,

and the assembly of tubulin was observed turbidimetrically. The IC_{50} value was defined as the compound concentration that inhibited the extent of assembly by 50% after 20 min incubation.

5.2.3. Flow cytometric analysis of cell cycle distribution—For flow cytometric analysis of DNA content, 5×10^5 HeLa or Jurkat cells in exponential growth were treated with different concentrations of the test compounds for 24 and 48 h. After the incubation, the cells were collected, centrifuged and fixed with ice-cold ethanol (70%). The cells were then treated with lysis buffer containing RNAse A and 0.1% Triton X-100 and then stained with PI. Samples were analyzed on a Cytomic FC500 flow cytometer (Beckman Coulter). DNA histograms were analyzed using Multi-Cycle® for Windows (Phoenix Flow Systems).

5.2.4. Annexin-V assay—Surface exposure of PS on apoptotic cells was measured by flow cytometry with a Coulter Cytomics FC500 (Beckman Coulter) by adding Annexin-V-FITC to cells according to the manufacturer's instructions (Annexin-V Fluos, Roche Diagnostic). Simultaneously the cells were stained with PI. Excitation was set at 488 nm, and the emission filters were at 525 nm and 585 nm, respectively.

5.2.5. Assessment of mitochondrial changes—The mitochondrial membrane potential was measured with the fluorescent dye rhodamine 123 (Rho 123, Pierce, Rockford IL, USA), as described [36]. Briefly, after different times of treatment, the cells were collected by centrifugation and resuspended in Hank's Balanced Salt Solution (HBSS) containing 0.1 μM Rho 123. The cells were then incubated for 20 min at 37 °C, centrifuged and resuspended in HBSS. The production of ROS was measured by flow cytometry using either HE (Molecular Probes) or H_2DCFDA (Molecular Probes). After different times of treatment, cells were collected by centrifugation and resuspended in HBSS containing the fluorescence probes HE or H_2DCFDA at the concentrations of 2.5 and 0.1 μM, respectively. The cells were then incubated for 30 min at 37 °C, centrifuged and resuspended in HBSS. The fluorescence was directly recorded with the flow cytometer, using as excitation wavelength 488 nm and emission at 585 nm and 530 nm for HE and H_2DCFDA, respectively.

5.2.6. Caspase-3 assay—Caspase-3 activation in Jurkat cells was evaluated by flow cytometry using a human active caspase-3 fragment antibody conjugated with FITC (BD Pharmingen). Briefly, after different incubation times in the presence of test compounds, the cells were collected by centrifugation and resuspended in Cytofix™ (BD Pharmingen) buffer for 20 min, washed with Perm/Wash™ (BD Pharmingen) and then incubated for 30 min with the antibody. After this period, cells were washed and analyzed by flow cytometry. Results are expressed as percentage of caspase-3 active fragment positive cells.

5.2.7. Western blot analysis—Jurkat cells were incubated in the presence of test compounds and, after different times, were collected, centrifuged and washed two times with ice-cold phosphate-buffered saline (PBS). The pellet was then resuspended in lysis buffer. After the cells were lysed on ice for 30 min, lysates were centrifuged at 15000×g at 4 °C for 10 min. The protein concentration in the supernatant was determined using BCA protein assay reagents (Pierce, Italy). Equal amounts of protein (20 μg) were resolved using sodium dodecyl sulfate polyacrylamide gel electrophoresis (SDS-PAGE) (7.5–15% acrylamide gels) and transferred to a PVDF Hybond-*p* membrane (GE Healthcare). Membranes were blocked with I-block (Tropix), the membrane being gently rotated overnight at 4 °C. Membranes were then incubated with primary antibodies against, Bcl-2, PARP, Cdc25C, Bax, and p53 (all rabbit, 1:1000, Cell Signaling, Milano, Italy), Cyclin B1 (mouse, 1:1000, BD, Milano Italy) or β-actin (mouse, 1:10,000, Sigma–Aldrich, Milano,

Italy) for 2 h at room temperature. Membranes were next incubated with peroxidase-labeled goat anti-rabbit IgG (1:100,000, Sigma–Aldrich) or peroxidase-labeled goat anti-mouse IgG (1:100,000, Sigma–Aldrich) for 60 min. All membranes were visualized using ECL Advance (GE Healthcare) and exposed to Hyperfilm MP (GE Healthcare). To ensure equal protein loading, each membrane was stripped and reprobed with anti-β-actin antibody.

Acknowledgments

The authors would like to thank Dr. Alberto Casolari for excellent technical assistance.

References

[1]. Amos LA. Microtubule structure and its stabilisation. Org. Biomol. Chem. 2004; 2:2153–2160. [PubMed: 15280946]

[2]. Walczak CE. Microtubule dynamics and tubulin interacting proteins. Curr. Opin. Cell. Biol. 2000; 12:52–56. [PubMed: 10679354]

[3]. Downing KH, Nogales E. Tubulin structure: insights into microtubule properties and functions. Curr. Opin. Struct. Biol. 1998; 8:785–791. [PubMed: 9914260]

[4]. Downing KH. Structural basis for the interaction of tubulin with proteins and drugs that affect microtubule dynamics. Annu. Rev. Cell. Dev. Biol. 2000; 16:89–111. [PubMed: 11031231]

[5]. Sorger PK, Dobles M, Tournebize R, Hyman AA. Coupling cell division and cell death to microtubule dynamics. Curr. Opin. Cell. Biol. 1997; 9:807–814. [PubMed: 9425345]

[6]. Mahindroo N, Liou JP, Chang JY, Hsieh HP. Antitubulin agents for the treatment of cancer. A medicinal chemistry update. Exp. Opin. Ther. Pat. 2006; 16:647–691.

[7]. Jordan MA, Wilson L. Microtubules as a target for anticancer drugs. Nat. Rev. Cancer. 2004; 4:253–265. [PubMed: 15057285]

[8]. Hadfield JA, Ducki S, Hirst N, McGown AT. Tubulin and microtubules as targets for anticancer drugs. Prog. Cell Cycle Res. 2003; 5:309–325. [PubMed: 14593726]

[9]. Honore S, Pasquier E, Braguer D. Understanding microtubule dynamics for improved cancer therapy. Cell. Mol. Life Sci. 2005; 62:3039–3065. [PubMed: 16314924]

[10]. Pellegrini F, Budman DR. Review: tubulin function, action of antitubulin drugs, and new drug development. Cancer Invest. 2005; 23:264–273. [PubMed: 15948296]

[11]. Attard G, Greystoke A, Kaye S, De Bono J. Update on tubulin binding agents. Pathol. Biol. 2006; 54:72–84. [PubMed: 16545633]

[12]. Beckers T, Mahboobi S. Natural semisynthetic and synthetic microtubule inhibitors for cancer therapy. Drugs Future. 2003; 28:767–785.

[13]. Hearn BR, Shaw SJ, Myles DC. Microtubule targeting agents. Compr. Med. Chem. 2007; 7:81–110.

[14]. Pettit GR, Singh SB, Hamel E, Lin CM, Alberts DS, Garcia-Kendall D. Isolation and structure of the strong cell growth and tubulin inhibitor combretastatin A-4. Experentia. 1989; 45:209–211.

[15]. Lin CM, Ho HH, Pettit GR, Hamel E. Antimitotic natural products combretastatin A-4 and combretastatin A-2: studies on the mechanism of their inhibition of the binding of colchicine to tubulin. Biochemistry. 1989; 28:6984–6991. [PubMed: 2819042]

[16]. Nam NH. Combretastatin A-4 analogues as antimitotic antitumor agents. Curr. Med. Chem. 2003; 10:1697–1722. [PubMed: 12871118]

[17]. Chaudari A, Pandeya SN, Kumar P, Sharma PP, Gupta S, Soni N, Verma KK, Bhardwaj G. Combretastain A-4 analogues as anticancer agents. Mini Rev. Med. Chem. 2007; 12:1186–1205.

[18]. Tron GC, Pirali T, Sorba G, Pagliai F, Busacca S, Genazzani A. Medicinal chemistry of combretastatin A4: present and future directions. J. Med. Chem. 2006; 49:3033–3044. [PubMed: 16722619]

[19]. Pinney KG, Bounds AD, Dingerman KM, Mocharla VP, Pettit GR, Bai R, Hamel E. A new anti-tubulin agent containing the benzo[b]thiophene ring system. Bioorg. Med. Chem. Lett. 1999; 9:1081–1086. [PubMed: 10328289]

[20]. Flynn BL, Verdier-Pinard P, Hamel E. A novel palladium-mediated coupling approach to 2,3-disubstituted benzo[b]thiophenes and its application to the synthesis of tubulin binding agents. Org. Lett. 2001; 3:651–654. [PubMed: 11259028]

[21]. Gaukroger K, Hadfield JA, Lawrence NJ, Nlan S, McGown AT. Structural requirements for the interaction of combretastatins with tubulin: how important is the trimethoxy unit? Org. Biomol. Chem. 2003; 1:3033–3037. [PubMed: 14518125]

[22]. Hatanaka T, Fujita K, Ohsumi K, Nakagawa R, Fukuda Y, Nihei Y, Suga Y, Akiyama Y, Tsuji T. Novel B-ring modified combretastatin analogues: synthesis and antineoplastic activity. Bioorg. Med. Chem. Lett. 1998; 8:3371–3374. [PubMed: 9873736]

[23]. Carrington DEL, Clarke K, Scrowston RM. 1,2-Benzisothiazoles. Part I. Reaction of 3-chloro-1,2-benzisothiazole with nucleophiles. J. Chem. Soc. 1971:3262–3265.

[24]. Beck JR. A facile synthesis of 2-phenylbenzo[b]thiophene-3-amine and the corresponding S-oxide. J. Heterocycl. Chem. 1978; 15:513–514.

[25]. Doyle MP, Siegfried B, Dellaria JF Jr. Alkyl nitrite-metal halide deamination reactions. 2. Substitutive deamination of arylamines by alkyl nitrites and copper (II) halides. A direct and remarkably efficient conversion of arylamines to aryl halides. J. Org. Chem. 1977; 42:2426–2431.

[26]. Shieh WC, Carlson JA. A simple asymmetric synthesis of 4-arylphenylalanines via palladium-catalyzed cross-coupling reaction of arylboronic acids with tyrosine triflate. J. Org. Chem. 1992; 57:379–381.

[27]. Queiroz M-JR, Begouin A, Ferreira ICFR, Kirsch G, Calhelha RC, Barbosa S, Estevinho LM. Palladium-catalysed amination of electron-deficient or relatively electron-rich benzo[b]thienyl bromides-preliminary studies of antimicrobial activity and SARs. Eur. J. Org. Chem. 2004:3679–3685.

[28]. Hooper MW, Utsunomiya M, Hartwig JF. Scope and mechanism of palladium-catalyzed amination of five-membered heterocyclic halides. J. Org. Chem. 2003; 68:2861–2873. [PubMed: 12662063]

[29]. Hamel E. Evaluation of antimitotic agents by quantitative comparisons of their effects on the polymerization of purified tubulin. Cell Biochem. Biophys. 2003; 38:1–21. [PubMed: 12663938]

[30]. Mollinedo F, Gajate C. Microtubules, microtubule-interfering agents and apoptosis. Apoptosis. 2003; 8:413–450. [PubMed: 12975575]

[31]. Clarke PR, Allan LA. Cell-cycle control in the face of damage – a matter of life or death. Trends Cell Biol. 2009; 19:89–98. [PubMed: 19168356]

[32]. Martin SJ, Reutelingsperger CP, McGahon AJ, Rader JA, van Schie RC, Laface DM, Green DR. Early redistribution of plasma membrane phosphatidylserine is a general feature of apoptosis regardless of the initiating stimulus: inhibition by overexpression of Bcl-2 and Abl. J. Exp. Med. 1995; 182:1545–1556. [PubMed: 7595224]

[33]. Vermes I, Haanen C, Steffens-Nakken H, Reutelingsperger C. A novel assay for apoptosis. Flow cytometric detection of phosphatidylserine expression on early apoptotic cells using fluorescein labelled annexin V. J. Immunol. Methods. 1995; 184:39–51. [PubMed: 7622868]

[34]. Green DR, Kroemer G. The pathophysiology of mitochondrial cell death. Science. 2005; 305:626–629. [PubMed: 15286356]

[35]. Ly JD, Grubb DR, Lawen A. The mitochondrial membrane potential (Δφm) in apoptosis: an update. Apoptosis. 2003; 3:115–128. [PubMed: 12766472]

[36]. Baracca A, Sgarbi G, Solaini G, Lenaz G. Rhodamine 123 as a probe of mitochondrial membrane potential: evaluation of proton flux through F0 during ATP synthesis. Biochim. Biophys. Acta Bioenerg. 2003; 1606:137–145.

[37]. Zamzami N, Marchetti P, Castedo M, Decaudin D, Macho A, Hirsch T, Susin SA, Petit PX, Mignotte B, Kroemer G. Sequential reduction of mitochondrial transmembrane potential and generation of reactive oxygen species in early programmed cell death. J. Exp. Med. 1995; 182:367–377. [PubMed: 7629499]

[38]. Nohl H, Gille L, Staniek K. Intracellular generation of reactive oxygen species by mitochondria. Biochem. Pharmacol. 2005; 69:719–723. [PubMed: 15710349]

[39]. Rothe G, Valet G. Flow cytometric analysis of respiratory burst activity in phagocytes with hydroethidine and 2′,7′-dichlorofluorescein. J. Leukoc. Biol. 1990; 47:440–448. [PubMed: 2159514]

[40]. Earshaw WC, Martins LM, Kaufmann SH. Mammalian caspases: structure, activation, substrates and functions during apoptosis. Annu. Rev. Biochem. 1999; 68:383–424. [PubMed: 10872455]

[41]. Denault J-B, Salvesen GS. Caspases: keys in the ignition of cell death. Chem. Rev. 2002; 102:4489–4499. [PubMed: 12475198]

[42]. Porter AG, Janicke RU. Emerging role of caspase-3 in apoptosis. Cell Death Differ. 1999; 6:99–104. [PubMed: 10200555]

[43]. Soldani C, Scovassi AI. Poly(ADP-ribose) polymerase-1 cleavage during apoptosis: an update. Apoptosis. 2002; 7:321–328. [PubMed: 12101391]

[44]. Kluck RM, Bossy-Wetzel E, Green DR. The release of cytochrome c from mitochondria: a primary site for Bcl-2 regulation of apoptosis. Science. 1997; 275:1132–1136. [PubMed: 9027315]

[45]. Knudson CM, Korsmeyer SJ. Bcl-2 and Bax function independently to regulate cell death. Nat. Genet. 1997; 16:358–363. [PubMed: 9241272]

[46]. Viola G, Fortunato E, Cecconet L, Del Giudice L, Dall'Acqua F, Basso G. Central role of p53 and mitochondrial damage in PUVA-induced apoptosis in human keratinocytes. Toxicol. Appl. Pharm. 2008; 227:84–96.

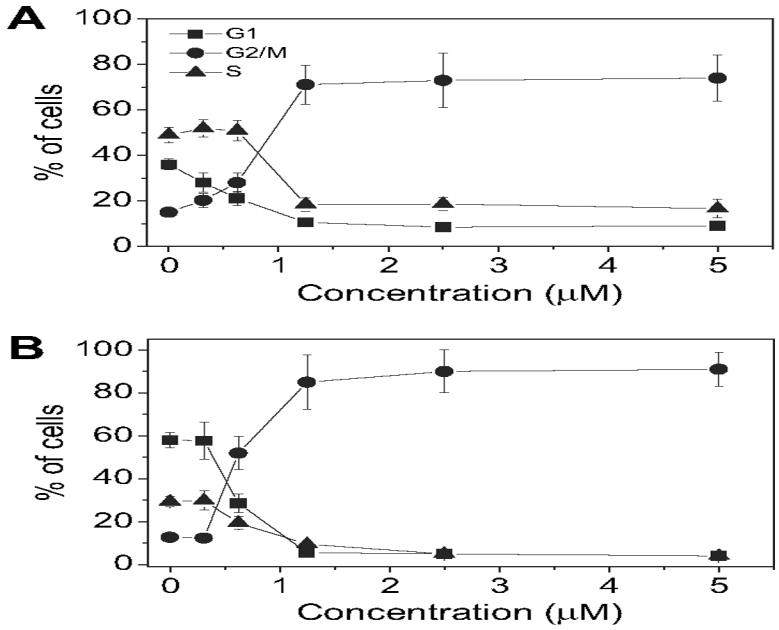

Fig. 1.

Effect of **4e**-induced G2/M phase arrest in Jurkat (panel A) and HeLa cells (panel B). Cells were treated with different concentrations ranging from 0.312 to 5 μM for 24 h. The cells were fixed and stained with PI to analyze DNA content by flow cytometry. Data are presented as mean ± SEM of two independent experiments.

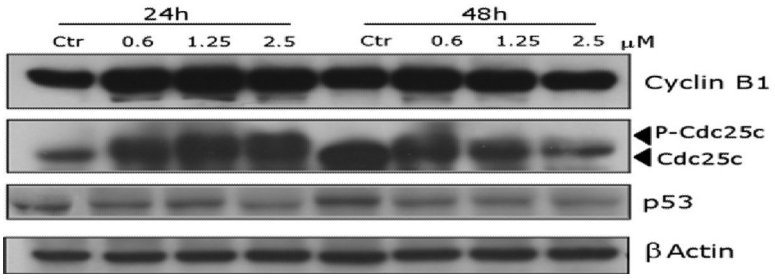

Fig. 2.

Effect of **4e** on the expression of cell cycle protein regulators. HeLa cells were treated for 24 or 48 h with the indicated concentration of the compound. The cells were harvested and lysed for the detection of cyclin B1, cdc25c and p53 expression by western blot analysis. To ensure equal protein loading, each membrane was stripped and reprobed with anti-β-actin antibody.

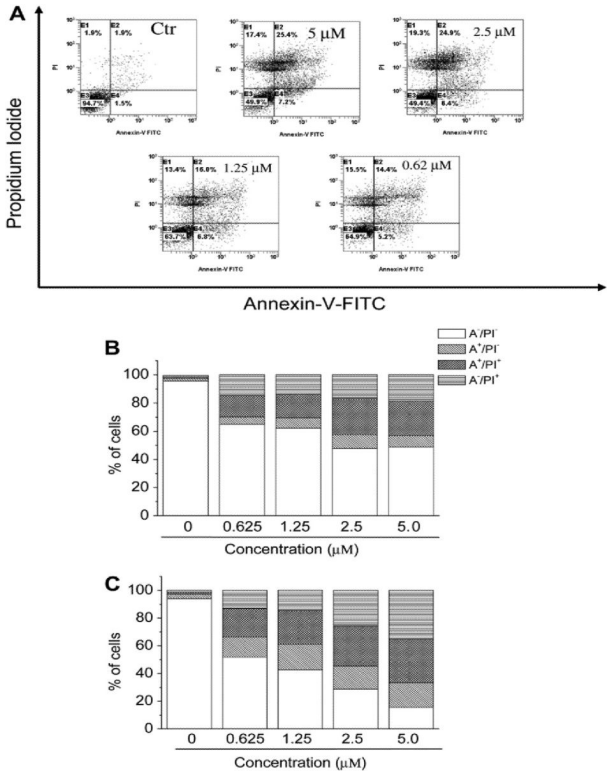

Fig. 3.

Flow cytometric analysis of apoptotic cells after treatment of HeLa cells with **4e**. The cells were harvested and labeled with annexin-V-FITC and PI and analyzed by flow cytometry. Panel A. Representative biparametric histograms obtained after 24 h of incubation at the indicated concentration of **4e**. In these histograms, the lower left-hand segment represents the annexin-V^-/PI^- cells, the lower right-hand segment the annexin-V^+/PI^- cells, the upper right-hand segment the annexin-V^+/PI^+ cells, and the upper left-hand segment the annexin-V^-/PI^+ cells. Panels B and C. Percentage of cells found in the different regions of the biparametric histograms shown in panel A, after incubation with **4e** for 24 h (panel B) and 48 h (panel C).

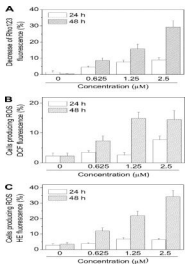

Fig. 4.

Assessment of mitochondrial dysfunction after treatment with compound **4e**. Panel A. Induction of loss of mitochondrial membrane potential after 24 and 48 h of incubation of HeLa cells with the indicated concentrations of **4e**. Cells were stained with the fluorescent probe Rho 123 and analyzed by flow cytometry. Data are expressed as mean ± S.E.M. of 3 independent experiments. Panels B and C. Mitochondrial production of ROS in HeLa cells. After 24 and 48 h of incubation with **4e** at the indicated concentrations, cells were stained with H_2-DCFDA (panel B) or HE (panel C) and analyzed by flow cytometry. Data are expressed as mean ± S.E.M. of three independent experiments.

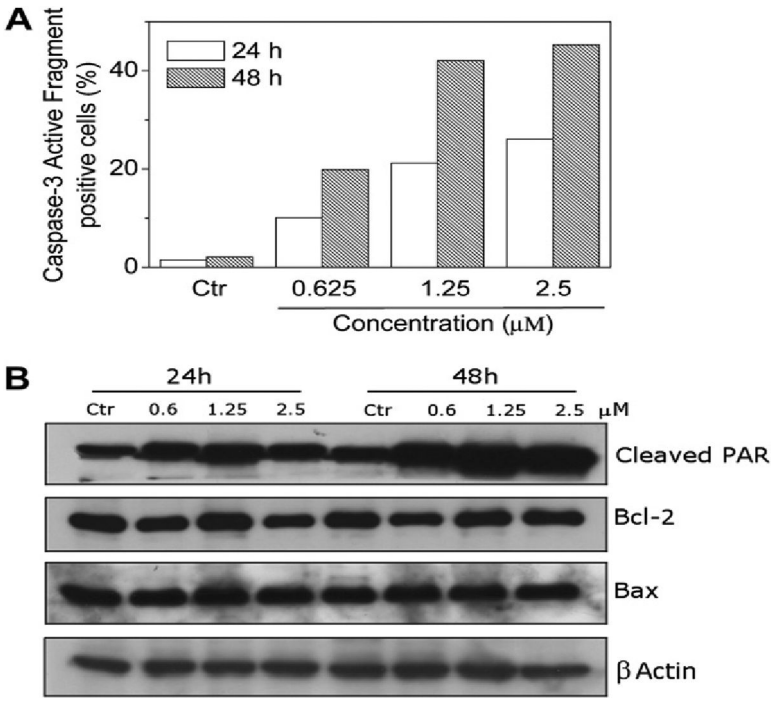

Fig. 5.

Panel A. Caspase-3 induced activity by compound **4e**. HeLa cells were incubated in the presence of **4e** at the indicated concentration. After 24 and 48 h of treatment, cells were harvested and stained with an anti-human active caspase-3 fragment monoclonal antibody conjugated with FITC. Data are expressed as percentage of Caspase-3 active fragment positive cells. Panel B. Western blot analysis for the cleavage of PARP and the expression of Bcl-2 and Bax in HeLa cells. Control lanes (Ctr) refer to untreated cells. In the other lanes the cell were treated with the indicated concentration of **4e** for the indicated times. Whole cell lysates were subjected to SDS-PAGE, followed by blotting with an anti-cleaved PARP (89 kDa), anti-Bcl-2, anti Bax or anti-actin antibody.

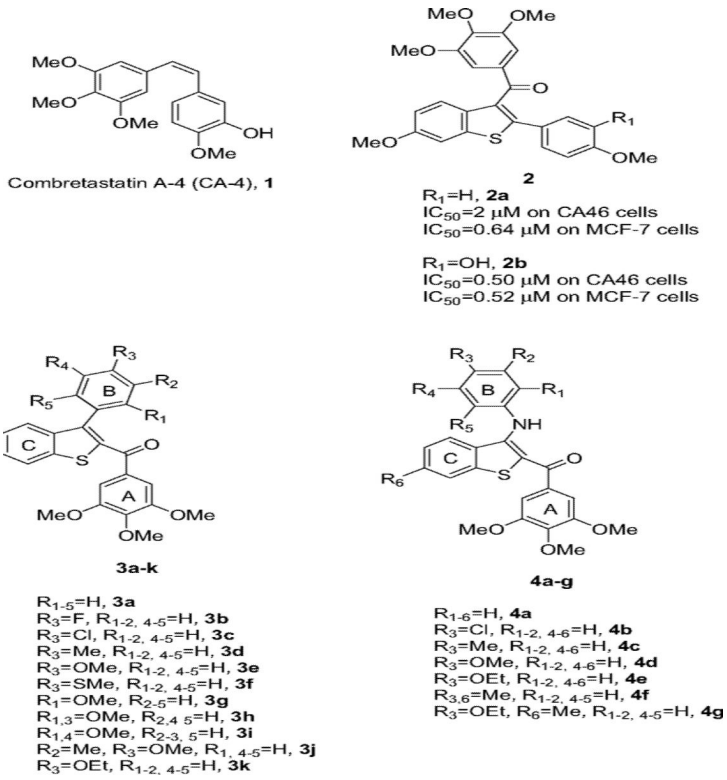

Chart 1.
Inhibitors of tubulin polymerization.

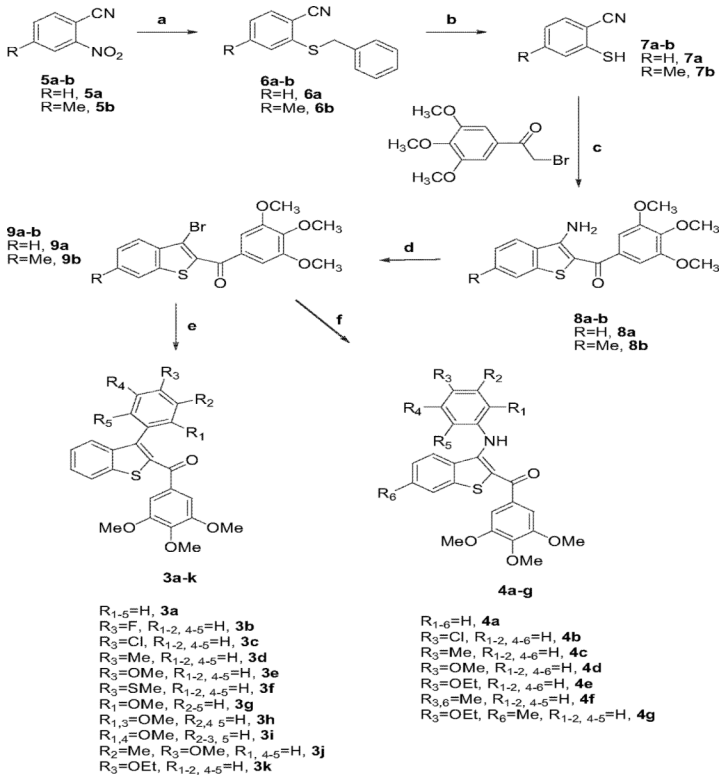

Scheme 1.

Reagents. a: $C_6H_5CH_2SH$, KOH, DMF; **b**: $AlCl_3$,C_6H_6; **c**: 3,4,5-trimethoxphenyl-2-bromoethanone, K_2CO_3, $(CH_3)_2CO$, rx, 18 h; **d**: t-BuONO, $CuBr_2$, CH_3CN, 65 °C; **e**: **9a**. $ArB(OH)_2$, $Pd(PPh_3)_4$, K_2CO_3, PhMe, rx, 18 h, **f**: **9a** or **9b**, $ArNH_2$, $Pd(OAc)_2$, BINAP, $CsCO_3$, PhMe, 100 °C, 16 h.

Table 1

In vitro antiproliferative effects of compounds **3a–k** and **4a–g**.

Compound	IC_{50}[a] (μM)				
	HeLa	A549	HL-60	Jurkat	K562
3a	1.9 ± 0.9	5.0 ± 0.9	1.7 ± 0.3	1.5 ± 0.5	2.1 ± 0.4
3b	3.0 ± 0.3	3.2 ± 0.4	3.2 ± 0.8	2.3 ± 0.9	2.1 ± 0.4
3c	5.2 ± 2.6	7.5 ± 0.7	3.3 ± 0.7	3.7 ± 0.8	4.2 ± 0.3
3d	3.7 ± 1.0	7.8 ± 0.8	1.4 ± 0.5	3.3 ± 1.0	3.5 ± 0.3
3e	4.2 ± 1.3	4.4 ± 0.5	1.6 ± 0.5	1.6 ± 0.6	1.7 ± 0.3
3f	3.5 ± 0.4	5.4 ± 0.5	1.3 ± 0.6	1.9 ± 0.2	1.8 ± 0.3
3g	5.0 ± 0.7	>10	2.9 ± 0.2	2.9 ± 0.3	3.4 ± 0.5
3h	3.9 ± 0.5	5.8 ± 0.5	4.6 ± 0.2	4.0 ± 0.2	4.1 ± 0.2
3i	>10	>10	>10	>10	>10
3j	>10	>10	>10	>10	>10
3k	3.0 ± 0.2	3.1 ± 0.05	3.5 ± 0.5	4.1 ± 0.5	3.1 ± 0.2
4a	2.7 ± 0.1	3.0 ± 0.2	5.2 ± 0.8	1.6 ± 0.8	2.3 ± 0.1
4b	3.7 ± 0.05	3.1 ± 0.1	5.4 ± 0.5	1.9 ± 0.1	1.1 ± 0.2
4c	3.5 ± 0.8	2.6 ± 0.3	4.6 ± 0.8	1.7 ± 0.5	1.6 ± 0.2
4c	7.7 ± 0.8	9.3 ± 0.9	3.7 ± 0.3	3.5 ± 0.8	2.9 ± 0.5
4c	0.7 ± 0.2	1.4 ± 0.2	0.5 ± 0.1	0.3 ± 0.1	0.2 ± 0.05
4f	0.98 ± 0.2	1.9 ± 0.4	1.9 ± 0.5	2.5 ± 0.8	1.4 ± 0.3
4g	4.3 ± 0.2	5.8 ± 0.2	4.0 ± 0.6	5.0 ± 0.4	4.3 ± 0.5

[a] IC_{50} = compound concentration required to inhibit tumor cell proliferation by 50%. Data are expressed as the mean ± SE from the dose-response curves of at least three independent experiments.